X-Band Wave Radar for Coastal Upwelling Detection off the Southern Coast of Sicily

F. RAFFA,[a] G. LUDENO,[b] B. PATTI,[c] F. SOLDOVIERI,[b] S. MAZZOLA,[c] AND F. SERAFINO[d]

[a] *Institute for Coastal Marine Environment, National Research Council (CNR-IAMC), Messina, Italy*
[b] *Institute for Electromagnetic Sensing of the Environment, National Research Council (CNR-IREA), Napoli, Italy*
[c] *Institute for Coastal Marine Environment, National Research Council (CNR-IAMC), Campobello di Mazara, Italy*
[d] *Institute of Biometeorology, National Research Council (CNR-IBMET), Florence, Italy*

(Manuscript received 22 February 2016, in final form 12 September 2016)

ABSTRACT

The main aim of this work is to show the potentialities of an X-band radar system about the detection of the coastal upwelling phenomenon. This is made possible by means of the estimation of the sea surface current, which moves from the coastal areas toward the open sea for wind-induced upwelling events. The study presents the results of the X-band radar data processing for a system installed at Capo Granitola (southwestern Sicily). In particular, the radar data acquired in three different periods—namely, 5–6 November 2013, 8–9 February 2015, and 6 March 2015—indicated upwelling events. The occurrence of these events was confirmed by independent information derived from in situ wind data provided by a meteorological station and the analysis of the satellite-derived sea surface temperature (SST) and chlorophyll-*a* (Chl-*a*) concentration.

1. Introduction

Coastal upwelling of deeper waters to the sea surface layer is a hydrological phenomenon with significant impact on the marine ecosystem (Smith 1968; Gill and Clarke 1974). The coastal wind-induced upwelling phenomenon consists of the replacement of the sea surface water, transported offshore due to the stress of the wind, with the water coming from the sea bottom. As upwelled water is colder and richer in macronutrients (nitrates, phosphates, and silicates) compared to the water usually present on the sea surface, the upwelling phenomenon has a significant impact on the marine environment because is able to boost both the primary and fish production in coastal Mediterranean areas generally characterized by highly oligotrophic conditions (Agostini and Bakun 2002; García Lafuente et al. 2002; Patti et al. 2004, 2008, 2010).

This paper is focused on the northern sector of the Strait of Sicily, where often a lower surface water temperature regime along the coast can be interpreted as a signature of the occurrence of upwelling events. Therefore, the difference of sea surface temperatures between an upwelling (coastal) zone and the surrounding (offshore) areas can represent a parameter suitable for detecting and characterizing the upwelling phenomenon. In particular, sea surface temperature variations can be observed from thermal satellite imagery, but the effectiveness of this remote sensing technique is limited by the weather conditions (clouds coverage). The same limitation also arises for the estimation of phytoplankton abundance (another indicator for the upwelling phenomenon), which can be derived by satellite-based imagery of chlorophyll-*a* concentration.

This paper shows the potential of an X-band radar system to detect an upwelling phenomenon through monitoring the sea surface current fields. In fact, one of the most significant effects of the wind-induced upwelling phenomenon is that sea surface current flows from the coastal areas toward the open sea. The main advantage of X-band radar systems relies on the capability to perform continuous time and all-weather measurements of the sea surface current, so as to monitor the upwelling phenomenon in real time. To confirm the reliability of the wave radar system to detect an upwelling phenomenon, a comparison is presented with independent information in terms of sea surface temperature variations, chlorophyll-*a* concentration, and an upwelling index based on wind data.

The paper is organized as follows. In section 2, the wind-induced coastal upwelling phenomenon is explained

Corresponding author e-mail: Bernardo Patti, bernardo.patti@cnr.it

DOI: 10.1175/JTECH-D-16-0049.1

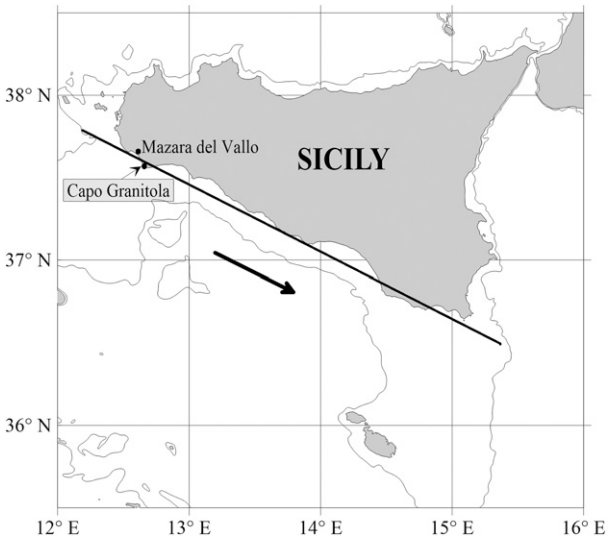

FIG. 1. Map showing the site of X-radar installation in the Strait of Sicily (Capo Granitola). The black line represents the northwest–southeast orientation of the southern Sicilian coastline, whereas the black arrow shows the direction of dominant winds (westerlies) able to induce coastal upwelling events in the area.

by Ekman's theory and the applied upwelling index is introduced. Section 3 reports briefly the X-band radar data processing exploited to estimate the surface currents. The outcomes achieved through the X-band radar system and their comparison with independent information provided by wind data and satellite-based observations are presented in section 4. Conclusions end the paper.

2. Offshore Ekman transport and its effect on the study area

The ocean surface water's net movement under the direct action of the wind (Ekman transport) is deflected by effects of the earth's rotation in a direction 90° to the right in the Northern Hemisphere (Ekman 1905).

On the Mediterranean Sea, the prevailing westerly winds produce offshore-directed Ekman transport, resulting in coastal upwelling off the southern sides of the bigger islands (Bakun and Agostini 2001; Agostini and Bakun 2002). In particular, several authors have reported a semipermanent coastal upwelling regime reinforced by local winds at the southern coast of Sicily (e.g., Salusti and Zambianchi 1985; Piccioni et al. 1988; Lermusiaux 1999; Robinson et al. 1999; Warn-Varnas et al. 1999; Lermusiaux and Robinson 2001; Molcard et al. 2002; Astraldi et al. 2002; Sorgente et al. 2003; Béranger et al. 2004; Poulain and Zambianchi 2007; Patti et al. 2010). Therefore, because of the northwest–southeast orientation of the southern coast of Sicily, winds from the northwest produce offshore transport in the upper layer, which can be considered an indicator of the amount of water upwelled along the coast (Mann and Lazier 1991). Therefore, for the southern coast of Sicily (see Fig. 1), when the wind direction is from the northwest, the combination of Ekman transport along the y axis (Q_y) with the Ekman transport along the x axis (Q_x) is a good indicator of upwelling intensity (enrichment processes). The opposite (downwelling) occurs when the wind direction is from the southeast.

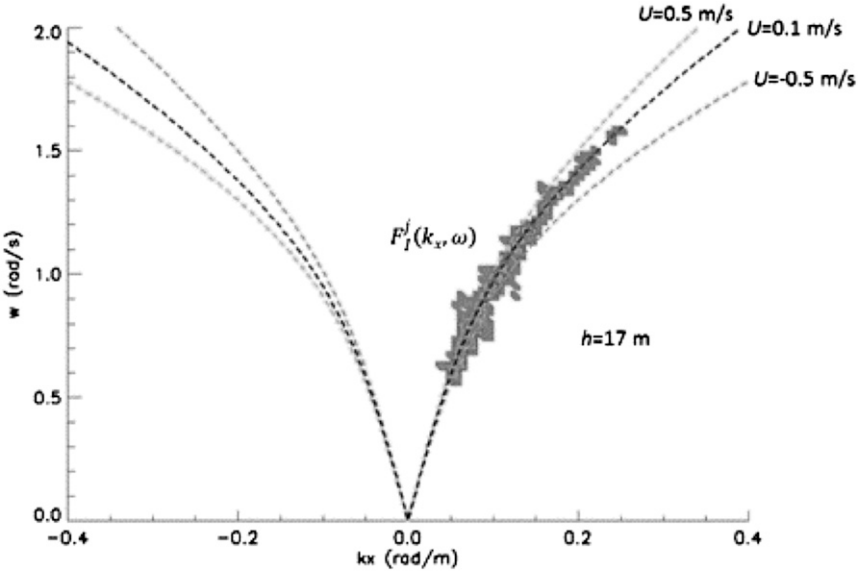

FIG. 2. 2D cut of the 3D radar image spectrum relevant to a sea patch with local bathymetry equal to 17 m and surface current amplitude equal to $U = 0.1\ \mathrm{m\ s^{-1}}$.

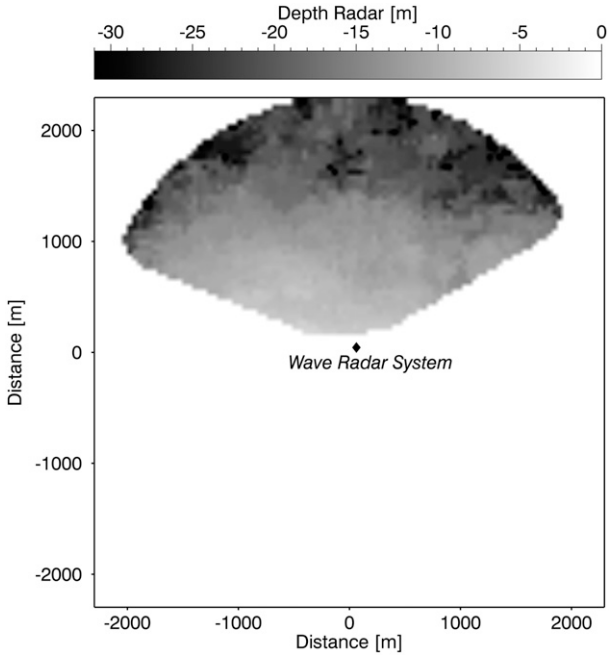

FIG. 3. Bathymetry map estimated during a previous measurements campaign.

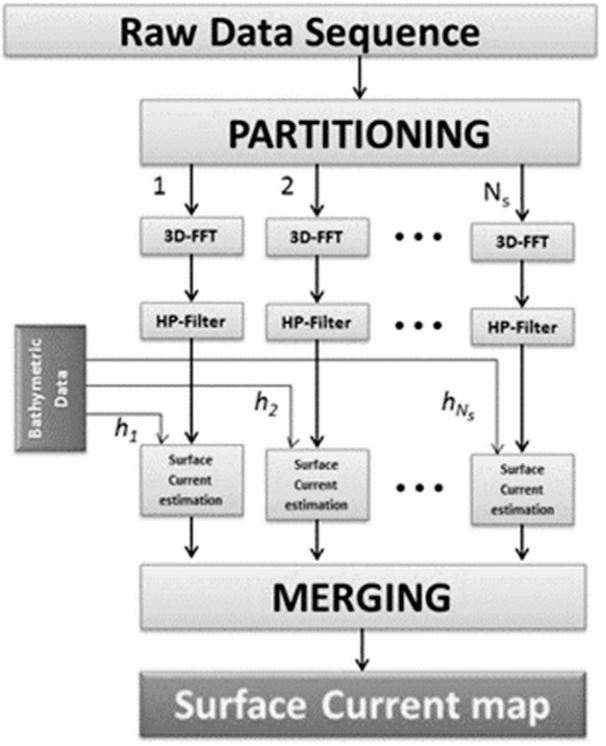

FIG. 4. Flowchart of the inversion procedure employed to reconstruct the sea surface current field from radar data.

Ekman transport components are evaluated according to Bakun (1973) and are defined as follows:

$$Q_x = \frac{\tau_y}{f_\rho}1000; \quad Q_y = \frac{-\tau_x}{f_\rho}1000, \tag{1}$$

where Q_x and Q_y are the Ekman transport components along the x (zonal) and y (meridional) axes, respectively ($m^3\,s^{-1}\,km^{-1}$); $\rho = 1025\,kg\,m^{-3}$ is the water density; f is the (latitude dependent) Coriolis factor (s^{-1}); and τ_x and τ_y are the wind stress components ($N\,m^{-2}$, i. e., $kg\,m^{-1}\,s^{-2}$) over the sea. Wind stress τ_x and τ_y values were calculated starting from the hourly instantaneous zonal (u) and meridional (v) components of wind values ($m\,s^{-1}$) using the following equations:

$$\tau_x = \rho_a C_d u\sqrt{u^2+v^2}; \quad \tau_y = \rho_a C_d v\sqrt{u^2+v^2}, \tag{2}$$

where $\rho_a = 1.2\,kg\,m^{-3}$(air density) and $C_d = 2.4\times10^{-3}$ (drag coefficient).

The analytic expression of the upwelling index (UI) is given by the following formulation:

$$\mathrm{UI} = Q_x \sin\theta + Q_y \cos\theta, \tag{3}$$

where $\theta = \phi - \pi/2$ and ϕ is the northwest–southeast coastline orientation with respect to north. In particular, for the investigated area (Capo Granitola harbor, see Fig. 1) ϕ is equal to 146°.

The upwelling index UI represents the module of the projection of vector $\mathbf{Q} = (Q_x, Q_y)$ along the direction perpendicular to the coastline and gives an indication of the wind-induced upwelling (negative values) or downwelling (positive values) events. For the sake of simplicity, in the graphs reported in the results section (section 4), the opposite of UI was used instead, and in the case of easterlies, the time series UI values were set to zero; in this way, positive values of UI indicate a wind regime inducing upwelling (westerlies) and zero values represent wind directions not inducing upwelling.

The wind data used to calculate the upwelling index were collected by the meteorological station of the Institute for Coastal Marine Environment of the National

TABLE 1. Measurement parameters of the wave radar system.

System parameters	Value
Antenna rotation period (Δt; s)	2.42
Spatial spacing of the images (Δx and Δy; m)	5.0
Minimum range (m)	250
Maximum range (m)	2309
Number of images per sequence (N)	32
Antenna height over sea level (m)	15
View angular sector (°)	110

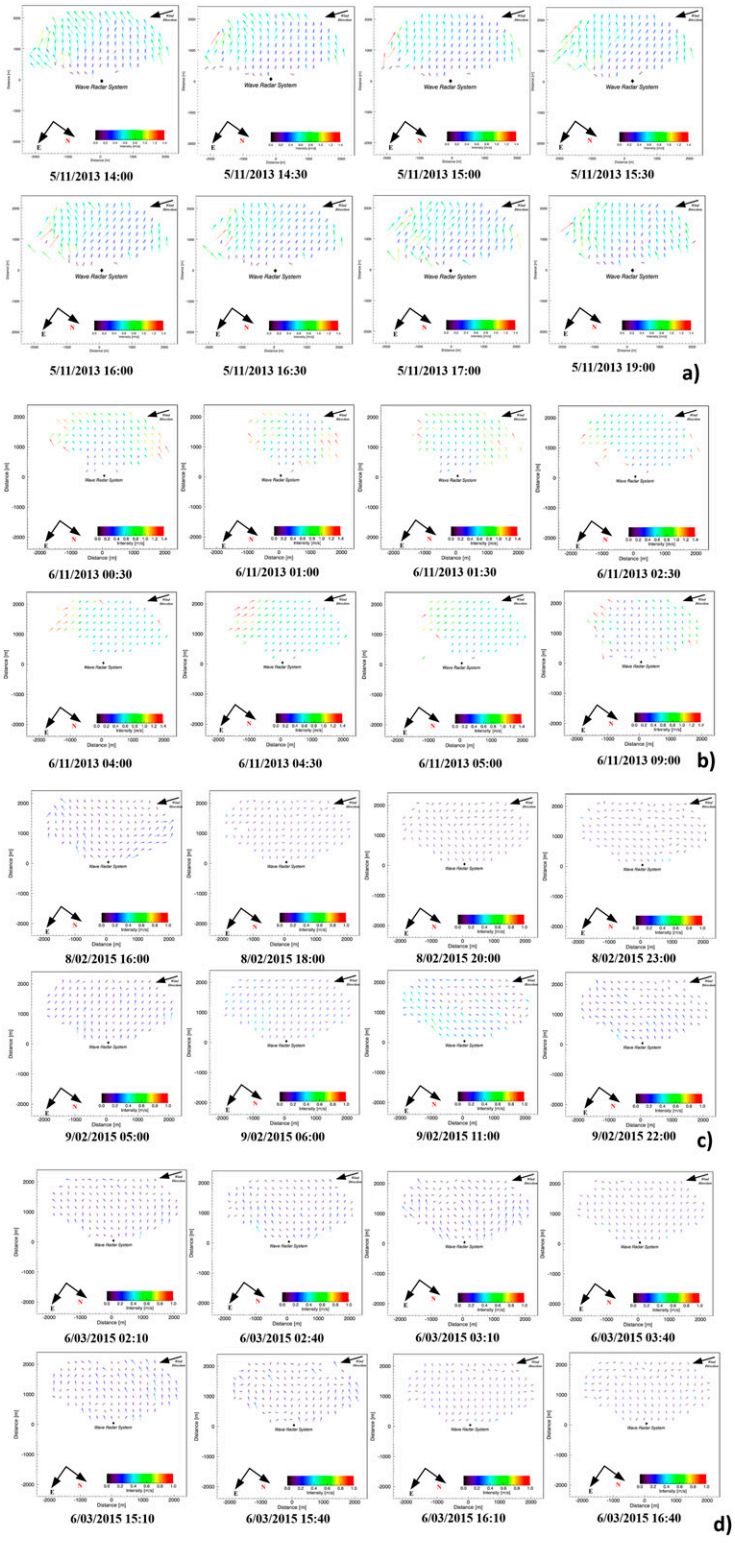

FIG. 5. Sea surface current fields that occurred at Capo Granitola during the periods (a) 1400–1900 UTC 5 Nov 2013, (b) 0030–0900 UTC 6 Nov 2013, (c) 8 (1600 UTC) and 9 (2200 UTC) Feb 2015, and (d) 0200–1640 UTC 6 Mar 2015.S.

TABLE 2. Mean surface current speed ($m\,s^{-1}$) and wind values ($m\,s^{-1}$) for the considered observation times.

5 Nov 2013			6 Nov 2013			8 and 9 Feb 2015			6 Mar 2015		
Time	U	Wind	Time	U	Wind	Time	U	Wind	Time	U	Wind
1400	0.44	14.8	0030	0.59	8.0	1600	0.12	3.8	0210	0.13	4.6
1430	0.45	15.2	0100	0.55	8.9	1800	0.13	0.3	0240	0.14	4.6
1500	0.45	15.2	0130	0.64	9.8	2000	0.10	2.4	0310	0.12	3.0
1530	0.46	14.8	0230	0.56	6.7	2300	0.10	4.6	0340	0.12	3.0
1600	0.47	12.5	0400	0.59	8.5	0500	0.16	4.2	1510	0.14	7.2
1630	0.47	12.5	0430	0.61	7.2	0600	0.21	2.4	1540	0.10	7.2
1700	0.50	11.6	0500	0.64	7.6	1100	0.24	5.6	1610	0.13	11.1
1900	0.60	14.0	0900	0.45	5.4	2200	0.13	8.2	1640	0.11	11.1

Research Council [L'Istituto per l'Ambiente Marino Costiero (IAMC) del Consiglio Nazionale delle Ricerche (CNR)] located in Capo Granitola, Sicily, when available, or otherwise by the meteorological station of Mazara del Vallo, at about 10 km from the experiment site (data available at http://www.sias.regione.sicilia.it/frameset_rete_new.htm).

3. X-band radar for upwelling detection and monitoring

X-band radars are gaining interest in the last decades because they are inexpensive and because of the wide scope of their application capabilities. In fact, the analysis of radar data allows us to retrieve useful information about the sea state, as for instance the direction, the period and the wavelength of the dominant waves, significant wave height, as well as surface current and bathymetry fields. The opportunity to estimate the sea current fields from radar data comes straight from the Doppler shift they cause on the wavenumber–frequency spectrum of the sea signals.

The propagation mechanisms of the sea gravity waves are indeed ruled by the dispersion relation

$$\omega(\mathbf{k}) = \sqrt{g|\mathbf{k}|\tanh(|\mathbf{k}|h)} + \mathbf{k}\cdot\mathbf{U}, \qquad (4)$$

which also defines the $\omega - k$ (spectral) domain where the sea energy concentrates. In Eq. (4), $\mathbf{k} = (k_x, k_y)$ represents the wave vector (whose magnitude $k = 2\pi/\lambda$ is the wavenumber, where λ is the wavelength), ω is the angular frequency related to the wave period T by ($\omega = 2\pi/T$), g represents the acceleration due to gravity, h is the bathymetry value, and $\mathbf{U} = (U_x, U_y)$ is the sea surface current.

Therefore, according to Eq. (4), a change in the sea current value turns into a linear drift of the spectral support of the sea signal, as shown in Fig. 2, where a 2D cut of the radar image spectrum measured from the radar in Capo Granitola is depicted. Therefore, the reconstruction of a sea current field can be carried out by estimating the dispersion relation from the 3D spectrum relevant to a sequence of radar images. In last three decades, several current and bathymetry measurements algorithms have been developed: least squares (LS) (Young et al. 1985), iterative least squares (ILS) (Senet et al. 2001), normalized scalar product (NSP) (Serafino et al. 2010a,b) and polar current shell (PCS) (Shen et al. 2015). In particular, in Huang and Gill (2012) the first three algorithms (LS, ILS, NSP) were compared with one another and an ADCP under low state. Among the three current algorithms used, the NSP method provided the best results in terms of

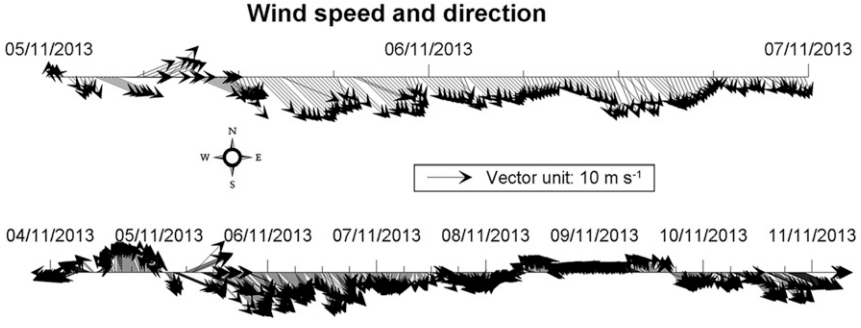

FIG. 6. Time series of wind speed and direction that occurred at Capo Granitola on (top) 5–6 Nov 2013 and (bottom) 4–10 Nov 2013.

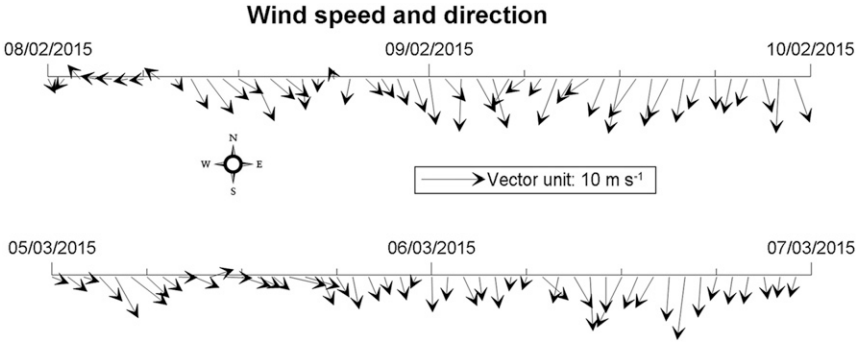

FIG. 7. Time series of wind speed and direction that occurred at the Mazara del Vallo meteorological station during the periods (top) 8–9 Feb 2015 and (bottom) 5–6 Mar 2015.

estimation accuracy and noise robustness. Moreover, in order to take into account the spatial nonuniformity of the surface current and bathymetry of the radar data acquired in the coastal area, several improved ''local'' inversion procedures have been developed (Senet et al. 2008; Hessner et al. 2014; Ludeno et al. 2014a). Herein, we adopt the ''local method'' based on the NSP method (Serafino et al. 2012; Ludeno et al. 2014a,b, 2016).

In particular, the NSP method is founded on the maximization of the normalized scalar product between the amplitude of the radar spectrum, here denoted with $|F_I(\mathbf{k}, \omega)|$, and the following characteristic function:

$$G(\mathbf{k},\omega,\mathbf{U},h) = \delta(\omega - \sqrt{g|\mathbf{k}|\tanh(|\mathbf{k}|h)} - \mathbf{k}\cdot\mathbf{U}), \quad (5)$$

which accounts for the local support of the dispersion relation. Accordingly, the NSP estimates $\hat{\mathbf{U}}$ of the surface currents arise from the following equation:

$$\hat{\mathbf{U}} = \arg\max_{\mathbf{U}} \frac{\langle |F_I(\mathbf{k},\omega)|, G(\mathbf{k},\omega,\mathbf{U},h)\rangle}{\sqrt{P_{F_I} P_G}}, \quad (6)$$

where $\langle |F_I(\mathbf{k}, \omega)|, G(\mathbf{k}, \omega, \mathbf{U}, h)\rangle$ denotes the scalar product between the functions $F_I(\cdot)$ and $G(\cdot)$, having a power equal to P_{F_I} and P_G, respectively. It is worth noting that the component $\hat{\mathbf{U}}$ estimated from the radar spectrum represents a weighted mean current over the upper layer of the ocean (Stewart and Joy 1974). In particular, it is defined as the summation of the tidal current U^t, the current associated with ocean circulations U^{os}, the wind drift current U^d, and the wave-induced current U^w (Young et al. 1985), $\hat{\mathbf{U}} = U^t + U^{os} + U^d + U^w$. (6) Moreover, the NSP method allows for, in principle, the joint estimation of the surface current and bathymetry values. In this work, we assume a priori information about the sea depth, which is provided by external data estimated during a previous measurements campaign (see Fig. 3). Nevertheless, a local estimation procedure based on the spatial partitioning of the radar images into partially overlapping patches allows us to benefit from NSP accuracy even in a coastal zone. However, the patch's extent does not infer the resolution of the sea surface current estimates, since the spatial details of the retrieved current maps depend on only the overlap between two contiguous patches. The flowchart of this estimation procedure is depicted in Fig. 4.

4. X-band radar monitoring results in relation to wind- and satellite-based data

The radar was installed on the top of a building at a height of 15 m above sea level and located at the following coordinates: 37°34′19.70″N, 12°39′33.45″E; see Fig. 1.

The marine radar deployed for the measurements is a Consilium X-band radar equipped with a 9-ft-long (2.7 m) antenna and is able to transmit a peak power of 25 kW with horizontal transmit and horizontal receive (HH) polarization. The marine radar was connected to the data processing and visualization unit, which incorporates an analog-to-digital (AD) converter for the received signal. The images were stored using a 13-bit unsigned integer format, on a Cartesian grid with 1024 × 1024 pixels. The wave radar system provided the estimates of the characteristic sea state parameters with a 30-min interval. Several details of the acquisition system are given in Table 1. Herein, we present the temporal sequence of the sea surface current fields that occurred at the Capo Granitola site during three different periods (5–6 November 2013, 8–9 February, and 6 March 2015) and that are depicted in Figs. 5a–d, respectively. These reconstructions clearly show that in the considered periods, the surface

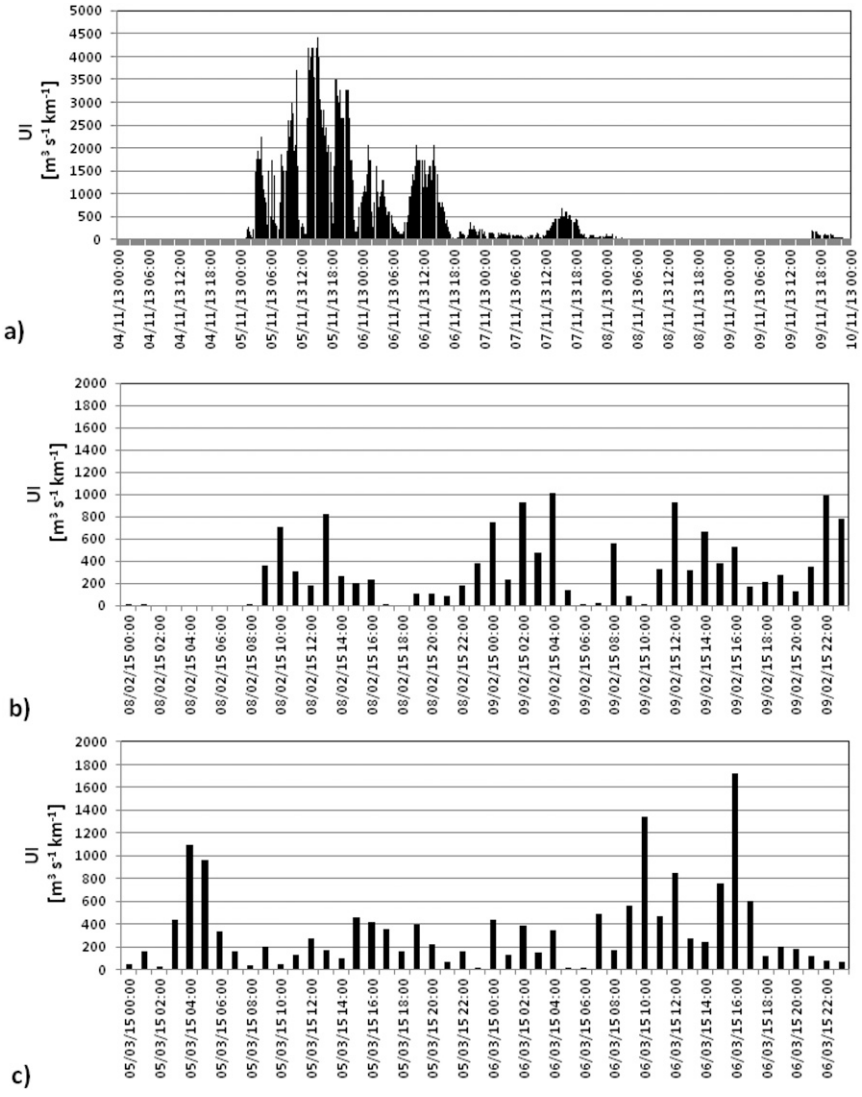

FIG. 8. Time series of upwelling index (a) from 4 (0015 UTC) to 14 Nov (1315 UTC) 2013, (b) 8 (0000 UTC) and 9 Feb (2300 UTC) 2015, and (c) 5 (0000 UTC) and 6 Mar (2300 UTC) 2015.

current flows from the coastline toward the open sea with an angle of about 45° with respect to the wind direction (west-northwest) according to Ekman's upwelling theory. The average intensity (in the range 0.10–0.64 m s^{-1}; see Table 2 and Figs. 6 and 7) is consistent with the observed wind forcing (Pugh 1987), which was lower in the two events that occurred in 2015 compared to the November 2013 event. This behavior has been interpreted as an indicator of the occurrence of upwelling events.

It is worth noting that for the study area, the major contribution in the Eq. (6) is given by wind drift U^d. In fact, in the Mediterranean Sea, the currents associated with ocean circulations U^{os} are relatively weak, especially along the coast and the tidal current U^t (Sorgente et al. 2003; Bonanno et al. 2014). The wave-induced currents U^w have a significant effect on the surfzone, that is, the nearshore zone where the waves come onto the beach (Michaud H. et al. 2012); anyway, our radar data do not cover the nearshore zone.

Since no independent measurements of sea surface currents (i.e., current measurements provided by other sensors) were available for the considered period, the possible presence of an upwelling phenomenon has been inferred by independent information provided by the measurement of the surface wind and the analysis of the sea surface temperature and the chlorophyll-*a* concentration satellite-based fields in the neighborhood of the

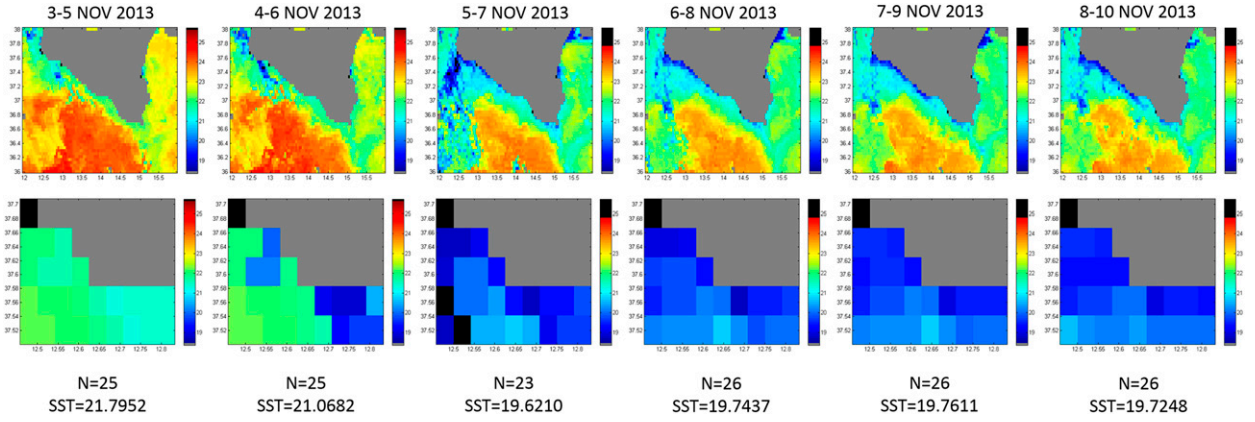

FIG. 9. SST 3-day average composite images for the period 3–10 Nov 2013. Box limits are (top) 32°–38°N, 12°–16°E, and (bottom) 37°30′–37°40′N, 12°30′–12°50′E; *N* stands for the number of pixels, gray pixels stand for the land, and black pixels are for the cloud cover.

experiment site. As shown hereafter, these independent observations provide evidence of a coastal upwelling phenomenon that occurred at Capo Granitola during the period 4–10 November 2013. Because of cloud coverage, for the periods 8–9 February 2015 and 6 March 2015, the occurrence of upwelling events was inferred by using wind data only. The next subsections show how the in situ wind data and the satellite-derived outcomes provide evidence of the upwelling phenomenon during the three considered periods.

a. The wind field data

Winds prevalently blow from northwest–north-northwest due to the typical weather conditions observed in the Mediterranean Sea, as observed in several papers (Piccioni et al. 1988; Korres et al. 2000; Zecchetto and Cappa 2001).

The local trend of the wind field in the neighborhood of the experiment site could be observed from the anemometer data collected by the meteorological station of the CNR-IAMC in Capo Granitola, when available, otherwise from the nearby meteorological station of Mazara del Vallo. In particular, the top panel of Fig. 6 reports the wind speed and direction observed at the Capo Granitola station on 5–6 November 2013, whereas the bottom panel shows the time series of the wind field that occurred in Capo Granitola on 4–10 November 2013. Figure 7 reports the time series of wind speed and direction collected by the Mazara del Vallo meteorological station during the periods 8–9 February 2015 and 5–6 March 2015.

These wind data represent crucial information for the correct interpretation of the surface current maps obtained during the upwelling period. As can be observed from the time series of Fig. 6, a sharp increase in the westerly wind intensity (up to 10–15 $\mathrm{m\,s^{-1}}$) occurred during 5–6 November 2013. A similar pattern was observed on 8–9 February 2015 and on 5–6 March 2015 but with lower wind speed values (Table 2; Fig. 7).

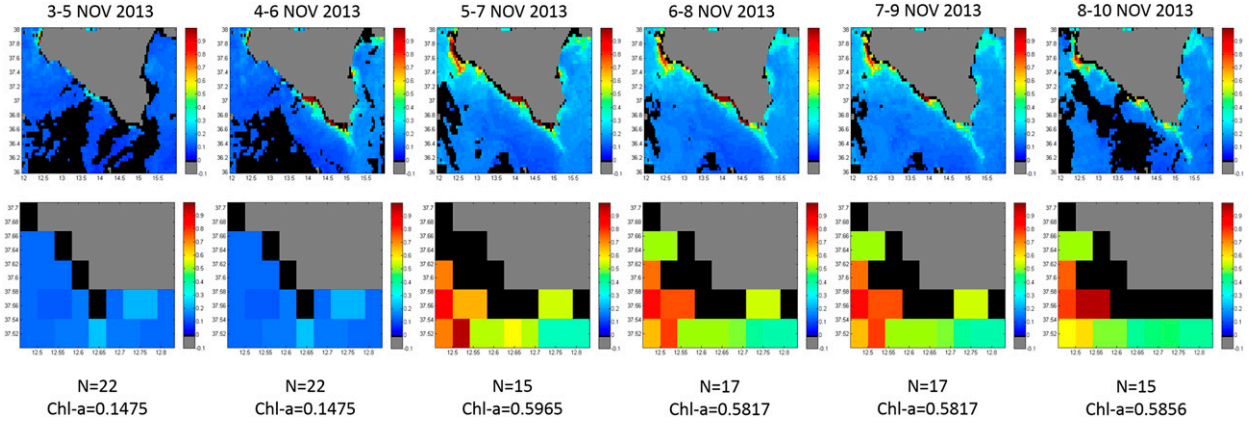

FIG. 10. Chl-*a* concentration 3-day average composite images for the period 3–10 Nov 2013, where *N* is the number of pixels, gray pixels stand for the land, and black pixels are for the cloud cover.

Figure 8 shows the hourly UI values during the periods 4–10 November 2013, 8–9 February 2015, and 5–6 March 2015, respectively. It is worth noting how the highest UI values (corresponding to westerly wind patterns) are consistent with the offshore-directed sea surface current estimated by X-band radar (Figs. 5a–d); a lower sea surface current speed occurred for the two 2015 events as expected due to the reduced wind forcing compared to the upwelling event that occurred in November 2013 (Table 2).

b. *SST and Chl-a in the Strait of Sicily*

Sea surface temperature (SST) and chlorophyll-*a* (Chl-*a*) concentration satellite-derived data used herein have been obtained from the Moderate Resolution Imaging Spectroradiometer (MODIS) aboard NASA's *Aqua* satellite, distributed as a level 3 standard mapped image product (Feldman and McClain 2006). Because of cloud coverage, satellite data were available only for the upwelling event that occurred in November 2013.

Specifically, 3-day composite images for the period 3–10 November 2013 were downloaded from online (http://oceancolor.gsfc.nasa.gov/cgi/l3) in Hierarchical Data Format (HDF). These images have 4320 × 8640 pixels and a pixel spacing of about 4 km × 4 km. From each downloaded image, the average SST and pigment concentration values were obtained for the area in front of the Capo Granitola station. The time behavior of the SST and Chl-*a* concentration (related to phytoplankton biomass) are shown in Figs. 9 and 10, respectively. Both parameters can be considered a signature of the effect of local favorable winds in the reinforcement of the upwelling regime in the study area.

Concerning the SST, an average temperature drop of about 2° (from 21.79° to 19.74°C) was registered in the considered area between 5 and 6 November 2013, while an increase of 0.45 $\mu g\,L^{-1}$ (from 0.14 to 0.59 $\mu g\,L^{-1}$) was observed in the Chl-*a* concentration on the same days. The evolution of both parameters (SST and the concentration of Chl-*a*) is consistent in providing evidence of the occurrence of a coastal upwelling event. This event was partially driven by the wind, since changes in SST and Chl-*a* were preceded by a consistent westerly wind pattern (about 24-h long) in the study area. Actually, in this season and in this area, subsurface waters are colder than the surface ones and also richer in macronutrients (nitrates, phosphates, silicates), which support the development of the phytoplankton biomass. So, coastal upwelling is expected to induce a decrease in SST and an increase in Chl-*a* concentration. In conclusion, the derived satellite data highly support the hypothesis of the occurrence of an upwelling event, most probably reinforced by favorable winds.

5. Conclusions

This study has shown the capabilities of X-band radar systems to detect the coastal upwelling phenomenon through the local monitoring of sea surface current fields. The latter opportunity could support many applications in marine ecology and fisheries science, since the coastal upwelling is closely related to primary production and, indirectly, to fish growth (Basilone et al. 2004) and fish biomass at sea (Levi et al. 2003; Patti et al. 2004). To investigate the relationship between the sea current estimated by the X-band radar and this important phenomenon, this study has analyzed the wind and sea temperature fields observed at Capo Granitola at the time of X-band radar observations. Future works will focus on the monitoring of the whole life cycle of the upwelling process.

Acknowledgments. The authors express their sincere appreciation to Dr. G. Frisone for his technical support to the scientific topic and to Dr. C. Angelica for the effort provided to the scientific data collection, to Mr. F. Cacciola for his work devoted to cataloging schematically the metadata, and to Mr. P. Calandrino for the dedicated collaboration. We also thank G. Tranchida for providing the wind data from the Capo Granitola weather station.

The research activity leading to this paper has been performed within the framework of the RITMARE Flagship Project, funded by the Italian Ministry of Education, University and Research (Grant 21023002).

REFERENCES

Agostini, V. N., and A. Bakun, 2002: 'Ocean Triads' in the Mediterranean Sea: Physical mechanisms potentially structuring reproductive habitat suitability (with example application to European anchovy, *Engraulis encrasicolus*). *Fish. Oceanogr.*, **11**, 129–142, doi:10.1046/j.1365-2419.2002.00201.x.

Astraldi, M., G. P. Gasparini, A. Vetrano, and S. Vignudelli, 2002: Hydrographic characteristics and interannual variability of water masses in the central Mediterranean: A sensitivity test for long-term changes in the Mediterranean Sea. *Deep-Sea Res. I*, **49**, 661–680, doi:10.1016/S0967-0637(01)00059-0.

Bakun, A., 1973: Coastal upwelling indices, west coast of North America, 1946-71. NOAA Tech. Rep. NMFS SSRF-671, 103 pp.

——, and V. Agostini, 2001: Seasonal patterns of wind driven upwelling/downwelling in the Mediterranean Sea. *Sci. Mar.*, **65**, 243–257, doi:10.3989/scimar.2001.65n3243.

Basilone, G., C. Guisande, B. Patti, S. Mazzola, A. Cuttitta, A. Bonanno, and A. Kallianiotis, 2004: Linking habitat conditions and growth in the European anchovy (*Engraulis encrasicolus*). *Fish. Res.*, **68**, 9–19, doi:10.1016/j.fishres.2004.02.012.

Béranger, K., L. Mortier, G. P. Gasparini, L. Gervasio, M. Astraldi, and M. Crèipon, 2004: The dynamics of the Sicily Strait: A comprehensive study from observations and models. *Deep-Sea Res. II*, **51**, 411–440, doi:10.1016/j.dsr2.2003.08.004.

Bonanno, A., and Coauthors, 2014: Variability of water mass properties in the Strait of Sicily in summer period of 1998–2013. *Ocean Sci.*, **10**, 759–770, doi:10.5194/os-10-759-2014.

Ekman, V. W., 1905: On the influence of the earth's rotation on ocean currents. *Ark. Mat. Astron. Fys.*, **2**, 1–55.

Feldman, G. C., and C. R. McClain, 2006: Ocean Color Web, MODIS Aqua. N. Kuring and S. W. Bailey, Eds., NASA Goddard Space Flight Center, accessed 23 April 2014. [Available online at http://oceancolor.gsfc.nasa.gov/cgi/l3.]

García Lafuente, J., A. García, S. Mazzola, L. Quintanilla, J. Delgado, A. Cuttitta, and B. Patti, 2002: Hydrographic phenomena influencing early stages of the Sicilian Channel anchovy. *Fish. Oceanogr.*, **11**, 31–44, doi:10.1046/j.1365-2419.2002.00186.x.

Gill, A. E., and A. J. Clarke, 1974: Wind-induced upwelling, coastal currents and sea-level changes. *Deep-Sea Res. Oceanogr. Abstr.*, **21**, 325–345, doi:10.1016/0011-7471(74)90038-2.

Hessner, K., K. Reichert, J. C. N. Borge, C. L. Stevens, and M. J. Smith, 2014: High-resolution X-band radar measurements of currents, bathymetry and sea state in highly inhomogeneous coastal areas. *Ocean Dyn.*, **64**, 989–998, doi:10.1007/s10236-014-0724-7.

Huang, W., and E. Gill, 2012: Surface current measurement under low sea state using dual polarized X-band nautical radar. *IEEE J. Sel. Top. Appl. Earth Obs. Remote Sens.*, **5**, 1868–1873, doi:10.1109/JSTARS.2012.2208179.

Korres, G., N. Pinardi, and A. Lascaratos, 2000: The ocean response to low-frequency interannual atmospheric variability in the Mediterranean Sea. Part I: Sensitivity experiments and energy analysis. *J. Phys. Oceanogr.*, **30**, 705–731, doi:10.1175/1520-0442(2000)013<0705:TORTLF>2.0.CO;2.

Lermusiaux, P. F. J., 1999: Estimation and study of mesoscale variability in the strait of Sicily. *Dyn. Atmos. Oceans*, **29**, 255–303, doi:10.1016/S0377-0265(99)00008-1.

——, and A. R. Robinson, 2001: Features of dominant mesoscale variability, circulation patterns and dynamics in the Strait of Sicily. *Deep-Sea Res. I*, **48**, 1953–1997, doi:10.1016/S0967-0637(00)00114-X.

Levi, D., and Coauthors, 2003: Embedding sea surface temperature anomalies into the stock recruitment relationship of red mullet (*Mullus barbatus* L. 1758) in the Strait of Sicily. *Sci. Mar.*, **67** (Suppl. 1), 259–268, doi:10.3989/scimar.2003.67s1259.

Ludeno, G., S. Flampouris, C. Lugni, F. Soldovieri, and F. Serafino, 2014a: A novel approach based on marine radar data analysis for high-resolution bathymetry map generation. *IEEE Geosci. Remote Sens. Lett.*, **11**, 234–238, doi:10.1109/LGRS.2013.2254107.

——, C. Brandini, C. Lugni, D. Arturi, A. Natale, F. Soldovieri, B. Gozzini, and F. Serafino, 2014b: Remocean system for the detection of the reflected waves from the Costa Concordia ship wreck. *IEEE J. Sel. Top. Appl. Earth Obs. Remote Sens.*, **7**, 3011–3018, doi:10.1109/JSTARS.2014.2321048.

——, C. Nasello, F. Raffa, G. Ciraolo, F. Soldovieri, and F. Serafino, 2016: A comparison between drifter and X-band wave radar for sea surface current estimation. *Remote Sens.*, **8**, 695, doi:10.3390/rs8090695.

Mann, K. H., and J. R. N. Lazier, 1991: *Dynamics of Marine Ecosystems: Biological–Physical Interactions in the Oceans*. 2nd ed. Blackwell Science, Inc., 466 pp.

Michaud, H., P. Marsaleix, Y. Leredde, C. Estournel, F. Bourrin, F. Lyard, C. Mayet, and F. Ardhuin, 2012: Three-dimensional modelling of wave-induced current from the surf zone to the inner shelf. *Ocean Sci.*, **8**, 657–681, doi:10.5194/os-8-657-2012.

Molcard, A., L. Gervasio, A. Griffa, G. P. Gasparini, L. Mortier, and T. M. Özgökmen, 2002: Numerical investigation of the Sicily Channel dynamics: Density currents and water mass advection. *J. Mar. Syst.*, **36**, 219–238, doi:10.1016/S0924-7963(02)00188-4.

Patti, B., and Coauthors, 2004: Interannual fluctuations in acoustic biomass estimates and in landings of small pelagic fish populations in relation to hydrology in the Strait of Sicily. *Chem. Ecol.*, **20**, 365–375, doi:10.1080/02757540410001727972.

——, and Coauthors, 2008: Factors responsible for the differences in satellite-based chlorophyll-a concentration between the major global upwelling areas. *Estuarine Coastal Shelf Sci.*, **76**, 775–786, doi:10.1016/j.ecss.2007.08.005.

——, C. Guisande, A. Bonanno, G. Basilone, A. Cuttitta, and S. Mazzola, 2010: Role of physical forcings and nutrient availability on the control of satellite-based chlorophyll *a* concentration in the coastal upwelling area of the Sicilian Channel. *Sci. Mar.*, **74**, 577–588, doi:10.3989/scimar.2010.74n3577.

Piccioni, A., M. Gabriele, E. Salusti, and E. Zambianchi, 1988: Wind-induced upwellings off the southern coast of Sicily. *Oceanol. Acta*, **11**, 309–314.

Poulain, P. M., and E. Zambianchi, 2007: Surface circulation in the central Mediterranean Sea as deduced from Lagrangian drifters in the 1990s. *Cont. Shelf Res.*, **27**, 981–1001, doi:10.1016/j.csr.2007.01.005.

Pugh, D. T., 1987: *Tides, Surges and Mean Sea-Level: A Handbook for Engineers and Scientisits*. Wiley, 472 pp.

Robinson, A. R., J. Sellschopp, A. Warn-Varnas, W. G. Leslie, C. J. Lozano, P. J. Haley Jr., L. A. Anderson, and P. F. J. Lermusiaux, 1999: The Atlantic Ionian Stream. *J. Mar. Syst.*, **20**, 129–156, doi:10.1016/S0924-7963(98)00079-7.

Salusti, E., and E. Zambianchi, 1985: Field observation of the onset of an upwelling on the Western Coast of Sicily during September 1984. *Boll. Oceanol. Teor. Appl.*, **3**, 299–308.

Senet, C. M., J. Seemann, and F. Ziemer, 2001: The near-surface current velocity determined from image sequences of the sea surface. *IEEE Trans. Geosci. Remote Sens.*, **39**, 492–505, doi:10.1109/36.911108.

——, ——, S. Flampouris, and F. Ziemer, 2008: Determination of bathymetric and current maps by the method DiSC based on the analysis of nautical X-band radar image sequences of the sea surface (November 2007). *IEEE Trans. Geosci. Remote Sens.*, **46**, 2267–2279, doi:10.1109/TGRS.2008.916474.

Serafino, F., C. Lugni, and F. Soldovieri, 2010a: A novel strategy for the surface current determination from marine X-Band radar data. *IEEE Geosci. Remote Sens. Lett.*, **7**, 231–235, doi:10.1109/LGRS.2009.2031878.

——, ——, J. C. Nieto Borge, V. Zamparelli, and F. Soldovieri, 2010b: Bathymetry determination via X-band radar data: A new strategy and numerical results. *Sensors*, **10**, 6522–6534, doi:10.3390/s100706522.

——, and Coauthors, 2012: REMOCEAN: A flexible X-band radar system for sea-state monitoring and surface current estimation. *IEEE Geosci. Remote Sens. Lett.*, **9**, 822–826, doi:10.1109/LGRS.2011.2182031.

Shen, C., W. Huang, E. W. Gill, R. Carrasco, and J. Horstmann, 2015: An algorithm for surface current retrieval from X-band marine radar images. *Remote Sens.*, **7**, 7753–7767, doi:10.3390/rs70607753.

Smith, R. L., 1968: Upwelling. *Oceanography and Marine Biology: An Annual Review*, Vol. 6, H. Barnes, Ed., Allen and Unwin, 11–46.

Sorgente, R., A. F. Drago, and A. Ribotti, 2003: Seasonal variability in the Central Mediterranean Sea circulation. *Ann. Geophys.*, **21**, 299–322, doi:10.5194/angeo-21-299-2003.

Stewart, R. H., and J. W. Joy, 1974: HF radio measurements of surface currents. *Deep-Sea Res. Oceanogr. Abstr.*, **21**, 1039–1049, doi:10.1016/0011-7471(74)90066-7.

Warn-Varnas, A., J. Sellschopp, P. J. Haley Jr., W. G. Leslie, and C. J. Lozano, 1999: Strait of Sicily water masses. *Dyn. Atmos. Oceans*, **29**, 437–469, doi:10.1016/S0377-0265(99)00014-7.

Young, I. R., W. Rosenthal, and F. Ziemer, 1985: A three-dimensional analysis of marine radar images for the determination of ocean wave directionality and surface currents. *J. Geophys. Res.*, **90**, 1049–1059, doi:10.1029/JC090iC01p01049.

Zecchetto, S., and C. Cappa, 2001: The spatial structure of the Mediterranean Sea winds revealed by ERS-1 scatterometer. *Int. J. Remote Sens.*, **22**, 45–70, doi:10.1080/014311601750038848.